UDC 629.785 EDN: OWONJP

FLIGHT CONTROL IN A HALO ORBIT IN VICINITY OF THE L2 POINT IN THE EARTH–MOON SYSTEM USING A SOLAR SAIL

W. Yu yussau@foxmail.com
O.L. Starinova solleo@mail.ru

Samara National Research University, Samara, Russian Federation

Abstract

In the context of the forthcoming Moon exploration and development initiatives, relay satellites for facilitating communication between the Earth and the Moon, particularly in regard to the far side and Polar Regions of the Moon, where permanent bases are planned, attract significant attention. This study focuses on the solar sails application in controlling motion of such relay satellites aimed at achieving efficient, precise, and long-term orbit keeping. A high-accuracy dynamic model of the spacecraft motion is created based on the ephemeris forecast of the celestial body motion, accompanied by the solar sail dynamic model with the controllable reflectivity. Using these models, the paper determines a reference halo orbit for the solar sail spacecraft in vicinity of the L2 point in the Earth–Moon system (EML2) through application of the multiple-shooting method. Subsequently, a solar sail control algorithm for tracking the reference orbit and applying the sliding mode method is developed, along with determination of the solar sail optimal parameters. A comparative analysis with the China's *Queqiao* relay satellite that utilizes chemical propulsion for the orbit keeping indicates that introduction of a solar sail could lead to the 66 % reduction in the fuel mass for orbit keeping, and achieving the comparable orbit keeping capabilities

Keywords

Relay satellite, halo orbit, solar sail, orbit keeping, multiple shooting method, sliding mode method

Received 05.03.2024
Accepted 10.03.2025

The work was financially supported by the China Scholarship Council

Introduction. In the imminent future, the Moon utilization and exploration would emerge as the focal point in the space exploration endeavors. Specifically, the far side and Polar Regions of the Moon are of particular attention. The far side of the Moon offers an electromagnetically interference-free environment

from the Earth, particularly advantageous in the deep space exploration [1]. Concentrated distribution of water in the lunar soils and ice further positions Polar Regions as suitable for establishing the permanent bases [2]. To date, the United States, Russia, the European Union, Japan, China, India, and South Korea are successfully launching spacecraft for the Moon exploration. Many of these spacecraft are not only exploring, but also landed on the far side or in the polar regions of the Moon. Their examples include the American Lunar Prospector, Lunar Reconnaissance Orbiter, LCROSS, Japanese Kaguya, Chinese Chang'e and the Indian Chandrayaan [3–7]. For the future, the United States is embarking on the Artemis project with the objective of deploying astronauts to the Moon's South Pole and establishing a permanent base [8]. Concurrently, China and Russia unveiled plans for an international lunar research station, and are inviting to participate in a myriad of the international scientific research projects [9, 10].

Successful implementation of these initiatives would require a multitude of satellites to ensure continuous relay communications between the Earth and the Moon. The most promising orbits for such satellites are the halo orbits around the EML2. Notably, the Chinese relay satellite *Queqiao-1* launched in June 2018 appears to be the first spacecraft to efficiently operate in such an orbit. *Queqiao-1* is an integral component of the Chang'e-4 project, which is aimed at studying the far side of the Moon. Another critical facet of the project is the *Yutu-2* lunar rover, i.e., the first probe to successfully land on the Moon's far side [11–15]. While operating in the halo orbit, *Queqiao-1* undergoes orbital adjustments approximately every 9.6 days facilitated by 4 hydrazine propulsion units with the 20N thrust and 20 units with the 5N thrust. The orbit keeping strategy involves applying an impulse, when the satellite traverses the xOz plane in the Earth–Moon synodic coordinate system plane (refer to Fig. 1) to ensure that the next time the satellite crosses the xOz plane from the same direction, the component velocity in the x direction equals zero. *Queqiao-1* was initially designed for the three-years' service life, during which 150 corrections were implemented, and 16.35 kg of fuel was consumed. After the entry in orbit, the anticipated service life was reevaluated and extended to 5 years. Leveraging high precision of the designed reference orbit, *Queqiao-1* still has enough fuel for keeping in orbit, and its operation is forecasted for a nine-years period. In anticipation of the upcoming Moon exploration projects, China planned to launch *Queqiao-2* in February 2024. The current launch plan was pushed forward to March.

Solar sail technology represents an innovative approach to space propulsion relying on the solar photons reflection and absorption to generate thrust.

Its primary advantage lies in the absence of fuel consumption theoretically enabling the unlimited momentum. However, a notable drawback is its limited thrust capability. For example, the maximum thrust that a 100 m^2 solar sail could produce is less than 0.9 mN. Pioneering success in the solar sail technology was demonstrated by the Japanese *Ikaros* project, which introduced a reflectivity control device to control thrust and orientation. This innovation facilitated controlled missions from the high Earth orbit to Venus and Mercury eliminating the need for traditional rockets. Achievements in the *Ikaros* project laid a crucial foundation for advancing the solar sail design and flight control [16, 17].

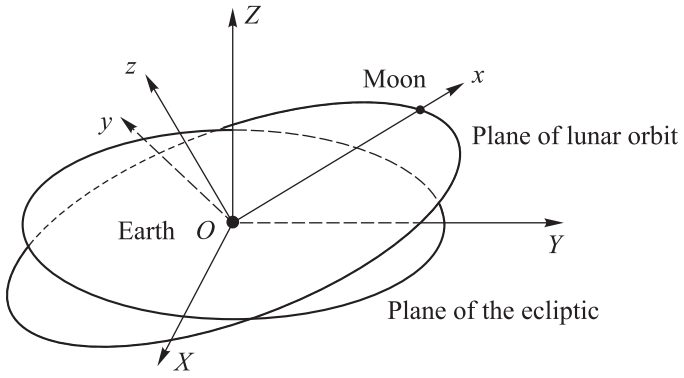

Fig. 1. J2000 inertial coordinate system $OXYZ$ and the Earth–Moon synodic coordinate system $Oxyz$

Based on the previous works in using solar sail for keeping an orbit, this article shifts the focus towards creating a high-precision reference halo orbit and meticulous selection of parameters for a spacecraft equipped with the solar sail [18–24].

Data and methods for solving problems, accepted assumptions. To depict motion of the celestial bodies and spacecraft, two coordinate systems are analyzed (see Fig. 1). The first is the J2000 inertial coordinate system $OXYZ$: the origin O is located at the center of the Earth; the axis OZ is perpendicular to the ecliptic plane at the moment J2000, as per the Julian calendar; the axis OX is directed towards the equinox at J2000; the axis OY is determined following the right-hand rule. The second is the Earth–Moon synodic coordinate system $Oxyz$: the axis Ox points towards the center of the Moon; the axis Oz coincides with the direction of the Moon's angular velocity around the Earth; the axis Oy is determined following the right-hand rule.

Neglecting all the disturbances and approximating the Earth and the Moon motion as the uniform circular motion around their common centers of mass, the spacecraft motion in the coordinate system $Oxyz$ could be represented

by a circular restricted three-body problem (CRTBP). In the CRTBP, halo orbits manifest as the periodic trajectories around the libration points. Let us express the spacecraft dynamic equation in the coordinate system as follows:

$$\dot{\mathbf{u}} = \mathbf{f}\left(\mathbf{u}\right), \tag{1}$$

where $\mathbf{u} = \left[x,\ y,\ z, v_x, v_y, v_z \right]^t$ is the state vector.

Approximate analytical solutions for the halo orbit could be derived by approximating the dynamic equation near the libration point using the Legendre series and solving it under the periodic constraints. However, this solution often is insufficient in forecasting the spacecraft trajectory with sufficient accuracy. For the enhanced precision, an iterative approach could be applied utilizing the differential correction method in conjunction with the state transition matrix until the desired accuracy is attained.

Let us consider the state vector at the initial moment t_0 denoted as $\mathbf{u}_0$, and at the final moment t_f denoted as $\mathbf{u}_f$. Clearly, $\mathbf{u}_f$ is a function of $\mathbf{u}_0$ and t_f:

$$\mathbf{u}_f = \psi\left(\mathbf{u}_0, t_f\right).$$

Taking a first-order variation of this equation, the following expression is obtained:

$$\delta\mathbf{u}_f = \mathbf{\Phi}\delta\mathbf{u}_0 + \dot{\mathbf{u}}_f\delta t,$$

where $\mathbf{\Phi}$ is the state transition matrix. The $\mathbf{\Phi}$ value could be found by integrating the following differential equation:

$$\dot{\mathbf{\Phi}} = \frac{\partial \mathbf{f}}{\partial \mathbf{u}^{\mathrm{T}}}\mathbf{\Phi}, \quad \mathbf{\Phi}\left(t_0\right) = \mathbf{I}_6,$$

where $\partial\mathbf{f} / \partial\mathbf{u}^t$ is the Jacobi matrix of $\mathbf{f}\left(\mathbf{u}\right)$ in (1); and $\mathbf{I}_6$ is the identity matrix.

Since the halo orbit is symmetrical relative to the plane xOz, and if at the initial moment the spacecraft is in the plane xOz, in that case $\mathbf{u}_0 = \left[x_0,\ 0,\ z_0,\ 0,\ v_{y0},\ 0 \right]^t$, the differential correction formula is transformed to the following form:

$$\begin{bmatrix} \delta x_0 \\ \delta v_{y0} \end{bmatrix} = \left(\begin{bmatrix} \Phi_{41} & \Phi_{45} \\ \Phi_{61} & \Phi_{65} \end{bmatrix} - \frac{1}{v_{yf}} \begin{bmatrix} v_{xf} \\ \dot{v}_{xf} \end{bmatrix} \begin{bmatrix} \Phi_{21} & \Phi_{25} \end{bmatrix} \right)^{-1} \begin{bmatrix} v_{xf} \\ v_{zf} \end{bmatrix}.$$

Iterating this formula several times enables derivation of the precise numerical solution for the halo orbit.

This solution is specifically tailored for the CRTBP. To extend its applicability to a reference orbit within the real force environment, it becomes imperative to construct a high-accuracy model detailing the spacecraft dynamics. In this comprehensive model, primary influence on the spacecraft motion arises from the gravitational forces exerted by various celestial bodies. In the coordinate system, the spacecraft acceleration due to gravity is equal to

$$\mathbf{g} = -\mu_e \frac{\mathbf{r}}{r^3} - \sum \mu_j \left(\frac{\mathbf{r}_j}{r_j^3} + \frac{\mathbf{R}_j}{R_j^3} \right),$$

where $\mathbf{r}$ is the vector of spacecraft position relative to the center of the Earth; $\mathbf{r}_j$ is the vector of spacecraft position relative to the center of the celestial body with index j; $\mathbf{R}_j$ is the vector of position of the j celestial body center relative to the center of the Earth, which is available through JPL ephemeris; μ_e and μ_j are the gravitational constants of the Earth and the j celestial body, respectively.

In the rotating coordinate system, the spacecraft dynamics equation has the form:

$$\ddot{\mathbf{r}} + 2\boldsymbol{\omega} \times \dot{\mathbf{r}} + \boldsymbol{\omega} \times \left(\boldsymbol{\omega} \times \mathbf{r} \right) + \dot{\boldsymbol{\omega}} \times \mathbf{r} = \mathbf{g} + \mathbf{a}_p, \tag{2}$$

where $\boldsymbol{\omega}$ is the coordinate system angular velocity, i.e., the angular Moon velocity around the Earth for $Oxyz$; $\mathbf{a}_p$ is the acceleration caused by forces other than the gravity. For a spacecraft with a solar sail, $\mathbf{a}_p$ is mainly caused by the sunlight pressure. Denoting vectors of the Moon position and velocity in the coordinate system $OXYZ$ as $\mathbf{R}_m$ and $\mathbf{V}_m$, the following expressions are obtained:

$$\boldsymbol{\omega} = \left[0, \quad 0, \quad \frac{\left| \mathbf{R}_m \times \mathbf{V}_m \right|}{\mathbf{R}_m^2} \right]^t;$$

$$\dot{\boldsymbol{\omega}} = \left[0, \quad \frac{\mathbf{R}_m \times \dot{\mathbf{V}}_m \left(\mathbf{R}_m \times \mathbf{V}_m \times \mathbf{R}_m \right)}{R_m^3 \left| \mathbf{R}_m \times \mathbf{V}_m \right|}, \quad \frac{\mathbf{R}_m \times \dot{\mathbf{V}}_m \left(\mathbf{R}_m \times \mathbf{V}_m \right)}{R_m^2 \left| \mathbf{R}_m \times \mathbf{V}_m \right|} \right]^t.$$

Figure 2 shows a kind of the solar sail with controllable reflectivity covered with the LCD panels.

When the LCD is on, it reflects light; when it is off, it absorbs light. By controlling the LCD area and position, the solar sail reflectivity and flipping torque could be controlled. For simplicity, this solar sail is conceptualized as reflecting a portion of the photon momentum completely and absorbing another portion completely. The diagram illustrating the sunlight impact on such a sail is presented in Fig. 3.

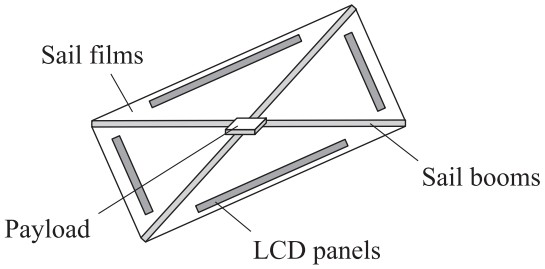

Fig. 2. Schematic diagram of a solar sail design with the controllable reflectivity

Fig. 3. Diagram of the sunlight impact on a solar sail with the controllable reflectivity

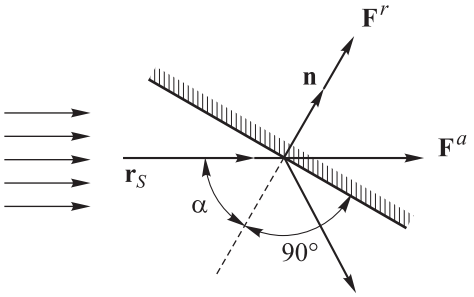

According to the Maxwell's light pressure equation

$$\mathbf{F}^r = 2\frac{\varepsilon}{c} S\left(\mathbf{r}_S\mathbf{n}\right)^2 \mathbf{n}; \quad \mathbf{F}^a = \frac{\varepsilon}{c} S\left(\mathbf{r}_S\mathbf{n}\right)\mathbf{r}_S;$$

$$\mathbf{a}_S = \frac{\mathbf{F}^a + \mathbf{F}^r}{m} = \kappa\left[\frac{u}{2}\left(\mathbf{r}_S\mathbf{n}\right)\mathbf{r}_S + \left(1-u\right)\left(\mathbf{r}_S\mathbf{n}\right)^2 \mathbf{n}\right],$$

where $\mathbf{r}_S$ is the sunlight direction vector; $\mathbf{n}$ is the solar sail normal direction vector; $\kappa = 2\varepsilon S/\mathrm{cm}$ is the maximum acceleration from light pressure. In the coordinate system with $\mathbf{r}_S$ and OZ as the coordinate axes:

$$\mathbf{a}_S = \kappa\frac{u}{2}\cos\alpha\left[1,\ \ 0,\ \ 0\right]^t + \kappa\left(1-u\right)\cos^2\alpha\left[\cos\alpha,\ \ \sin\alpha\sin\gamma,\ \ \sin\alpha\cos\gamma\right]^t; \quad (3)$$

$$\mathbf{a}_p = \mathbf{ABa}_S,$$

where $\mathbf{A}$ is the transformation matrix from the coordinate system $OXYZ$ to the coordinate system $Oxyz$; $\mathbf{B}$ is the transformation matrix from the coordinate system with $\mathbf{r}_S$ and OZ as the coordinate axes to the coordinate system $OXYZ$

$$\mathbf{A} = \left[\frac{\mathbf{R}_m}{R_m},\ \ \frac{\mathbf{R}_m\times\mathbf{V}_m\times\mathbf{R}_m}{\left|\mathbf{R}_m\times\mathbf{V}_m\right|R_m},\ \ \frac{\mathbf{R}_m\times\mathbf{V}_m}{\left|\mathbf{R}_m\times\mathbf{V}_m\right|}\right]^t;$$

$$\mathbf{B} = \left[-\frac{\mathbf{R}_S}{R_S},\ \ -\frac{\mathbf{R}_m\times\mathbf{V}_m\times\mathbf{R}_S}{\left|\mathbf{R}_m\times\mathbf{V}_m\right|R_S},\ \ \frac{\mathbf{R}_S}{R_S}\times\frac{\mathbf{R}_m\times\mathbf{V}_m\times\mathbf{R}_S}{\left|\mathbf{R}_m\times\mathbf{V}_m\right|R_S}\right]^t.$$

Here $\mathbf{R}_S$ is the Sun position vector in the coordinate system $OXYZ$.

As a result, a high-precision dynamics model is developed [2] for a spacecraft equipped with the solar sail, accounting for the forecasted celestial bodies' motion based on the ephemeris. Leveraging this model makes it possible to establish the reference orbits within the real force environment.

To establish the reference orbit for a spacecraft equipped with the solar sail, the multiple shooting method is applied.

In the multiple shooting method, first, moments t_0, t_1, t_2, …, t_n in the initial approach orbit are selected, i.e., numerical solution to the halo orbit and the corresponding motion state vectors are denoted as $\mathbf{u}_0$, $\mathbf{u}_1$, $\mathbf{u}_2$, …, $\mathbf{u}_n$. Then, starting from each moment t_k and ending at the next moment t_{k+1}, the motion state vectors $\psi(\mathbf{u}_k)$ and the corresponding state transition matrices $\mathbf{\Phi}_k$ are computed under constraint of the differential equation. Finally, state vectors satisfying the boundary conditions $\psi(\mathbf{u}_k) = \mathbf{u}_{k+1}$ are computed for all the moments. Consequently, all the segmented trajectories are seamlessly connected forming a continuous trajectory within constraints of the differential equation. The iterative formula for computing the motion state vectors takes the following form:

$$\begin{bmatrix} \mathbf{u}_1^{i+1} - \mathbf{u}_1^i \\ \mathbf{u}_2^{i+1} - \mathbf{u}_2^i \\ \vdots \\ \mathbf{u}_n^{i+1} - \mathbf{u}_n^i \end{bmatrix} = \begin{bmatrix} \mathbf{\Phi}_1 & -\mathbf{I} & \mathbf{0} & \cdots & \mathbf{0} \\ \mathbf{0} & \mathbf{\Phi}_2 & -\mathbf{I} & \cdots & \mathbf{0} \\ \vdots & \vdots & \ddots & \ddots & \vdots \\ \mathbf{0} & \mathbf{0} & \cdots & \mathbf{\Phi}_{n-1} & -\mathbf{I} \end{bmatrix}^{-1} \begin{bmatrix} \mathbf{u}_2^i - \psi(\mathbf{u}_1^i) \\ \mathbf{u}_3^i - \psi(\mathbf{u}_2^i) \\ \vdots \\ \mathbf{u}_n^i - \psi(\mathbf{u}_{n-1}^i) \end{bmatrix},$$

where $\mathbf{u}_k^i$ is the state vector of the k point in the i iteration cycle; $\psi(\mathbf{u}_k^i)$ is the state vector integrated from $\mathbf{u}_k^i$; $\mathbf{\Phi}_k$ is the transition matrix of states from k point to $k+1$ point. By iterating this formula several times, an exact numerical solution to the reference orbit for a spacecraft with the solar sail could be obtained.

Ensuring the spacecraft keeping orbit requires regulating the solar sail orientation angles α and γ, along with the reflectivity coefficient u in (3). Due to substantial nonlinearity of the solar sail dynamics equation, the control strategy should be adaptive to a broad range of the altering control variables. This paper applies a real-time control strategy based on the adaptive sliding mode method.

The sliding mode control concept is defined as follows: when the controlled object trajectory intersects with the sliding surface, the control force is applied to guide the trajectory back to the desired one. The sliding mode method relies on identifying the difference between the actual motion and the in-reference-orbit motion. The sliding surface developed in this paper is

$$\mathbf{S} = \mathbf{r} - \mathbf{r}_0 + \mathbf{\Gamma}\left(\dot{\mathbf{r}} - \dot{\mathbf{r}}_0\right),$$

where $\mathbf{r}_0$ is the reference orbit position vector; $\mathbf{\Gamma}$ is the velocity deviation weight matrix. The Lyapunov function is defined in the following form:

$$V = \frac{1}{2}\mathbf{S}^t\mathbf{S}.$$

According to (2), the control law is selected in the following form:

$$\mathbf{a}_p = \ddot{\mathbf{r}}_0 + 2\boldsymbol{\omega}\times\dot{\mathbf{r}} + \boldsymbol{\omega}\times\left(\boldsymbol{\omega}\times\mathbf{r}\right) + \dot{\boldsymbol{\omega}}\times\mathbf{r} - \mathbf{g} - \mathbf{\Gamma}^{-1}\left(\boldsymbol{\sigma}\mathbf{S} + \dot{\mathbf{r}} - \dot{\mathbf{r}}_0\right). \qquad (4)$$

Here $\boldsymbol{\sigma}$ represents the convergence rate matrix. Applying the control law to the system, the Lyapunov function derivative turns to be

$$\dot{V} = \mathbf{S}^t\dot{\mathbf{S}} = \mathbf{S}^t\left[\dot{\mathbf{r}} - \dot{\mathbf{r}}_0 + \mathbf{\Gamma}\left(\ddot{\mathbf{r}} - \ddot{\mathbf{r}}_0\right)\right] = -\mathbf{S}^t\boldsymbol{\sigma}\mathbf{S} < 0.$$

Thus, the Lyapunov function V is positive, and its derivative $\dot{V}$ is negative indicating that the system is asymptotically stable. Utilizing (3) and (4), values of the control variables $0 \le \alpha \le 90°$, $-180° \le \gamma \le 180°$, $0 \le u \le 1$ could be derived. By implementing the control law (4), the spacecraft could achieve the precise real-time tracking of the reference orbit.

In practical applications for simplification, the solar sail control variables should remain constant during the spacecraft flight in the reference orbit, $\alpha = \alpha_0$, $\gamma = \gamma_0$, $u = u_0$. Various values of these variables lead to the distinct reference orbits and exert an impact on the control strategy efficiency.

Results. Let us rewrite (4) in the following form $\mathbf{a}_p - \mathbf{a}_{p0} = \mathbf{F}\left(\mathbf{r}\right) - \mathbf{F}\left(\mathbf{r}_0\right)$, where

$$\mathbf{F}\left(\mathbf{r}\right) = 2\boldsymbol{\omega}\times\dot{\mathbf{r}} + \boldsymbol{\omega}\times\left(\boldsymbol{\omega}\times\mathbf{r}\right) + \dot{\boldsymbol{\omega}}\times\mathbf{r} - \mathbf{g} - \mathbf{\Gamma}^{-1}\left(\boldsymbol{\sigma}\mathbf{r} + \boldsymbol{\sigma}\mathbf{\Gamma}\dot{\mathbf{r}} + \dot{\mathbf{r}}\right);$$

$$\mathbf{a}_{p0} = \mathbf{a}_p\left(\alpha_0,\ \gamma_0,\ u_0\right).$$

The $\mathbf{a}_p - \mathbf{a}_{p0}$ value determines the control system ability to track the reference orbit when applying the developed control strategy. Given the stochastic nature of the disturbance direction, it is desirable for the solar sail to exhibit comparable control capabilities in all the directions. Coordinate transformation retains relative positions of coordinate points, and enables determination of the α_0, γ_0 and u_0 values by analyzing distribution of the $\mathbf{a}_S$ values. Figure 4 illustrates the $\mathbf{a}_S = \left[a_x,\ a_y,\ a_z\right]^t$ configuration for all three control variables values. It could be seen that the $\mathbf{a}_S$ values distribution demonstrates rotational symmetry around the a_x axis. Therefore, Fig. 4 focuses solely on the section composed of the a_x and a_y axes.

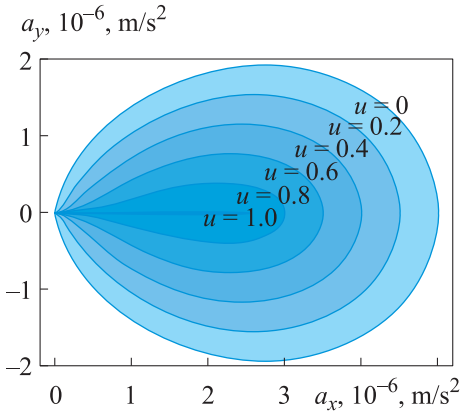

Fig. 4. Distribution of values $\mathbf{a}_S$ for all the values of α, γ and u (maximum acceleration $\kappa = 5 \cdot 10^{-6}$ m/s^2)

It becomes evident from the Fig. 4 that the $\mathbf{a}_S$ values spectrum encompasses all the points enclosed by the plane. After adding $\mathbf{a}_{S0}$, the $\mathbf{a}_S - \mathbf{a}_{S0}$ origin should be approximately equidistant from each point on the surface $u = 0$. Consequently, the point on axis a_x is designated corresponding to the highest value in the a_y direction as the new coordinate origin. Based on (3), the following expression is derived:

$$\alpha_0 = 0, \quad \gamma_0 = 0, \quad u_0 = 2\left(1 - \frac{2\sqrt{6}}{9}\right) \approx 0.91. \tag{5}$$

Main parameters of the *Queqiao-1* relay satellite are presented below:

Payload weight, kg	343.7
Fuel weight, kg	105
Fuel weight for keeping in orbit, kg	52.4
$\mathbf{a}_S - \mathbf{a}_{S0}$ consumed annually for keeping in orbit, m/s	36

Analyzing the data enables computation of the average disturbance acceleration that *Queqiao-1* could withstand in its reference orbit estimated to be approximately $\frac{\Delta v}{\Delta t} = \frac{36 \text{ m/s}}{365.24 \cdot 24 \cdot 3600 \text{ s}} = 1.14 \cdot 10^{-6}$ m/s^2. Figure 4 demonstrates that when maximum acceleration of the solar sail satellite is $\kappa = 5 \cdot 10^{-6}$ m/s^2, a similar disturbance withstanding capability to that of *Queqiao-1* could be achieved with a certain margin. At this point, the area-to-mass ratio of the solar sail satellite is $S/m = \kappa c/(2\varepsilon) = 0.56$ m^2/kg. Assuming that the solar sail satellite payload is the same as that of *Queqiao-1*, and the sail density matches that of *Ikaros* at 14 m · 14 m/16 kg, the required sail area would be 200 m^2. Consequently, parameters for the solar sail relay satellite could be determined in line with specifications provided below:

Payload weight, kg	343.7
Sail area, m^2	200
Sail weight, kg	17.8
Sail area to satellite mass ratio, m^2/kg	0.56

With parameters in (5) in any direction, maximum value of the correction acceleration $\mathbf{a}_S - \mathbf{a}_{S0}$ that the solar sail could create is $1.93 \cdot 10^{-6}$ m/s^2. Using the multiple shooting method, the reference halo orbit could be obtained for a spacecraft with the solar sail, as shown in the Fig. 5.

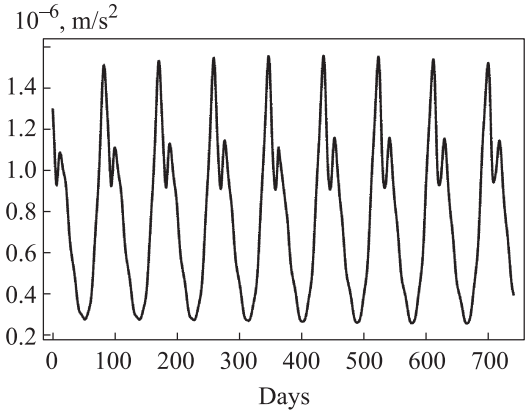

Fig. 5. Reference halo orbit of a spacecraft with the solar sail (the coordinates origin is at EML2)

In case the disturbance acting on the spacecraft from factors like precision of the reference orbit design, errors during the orbital entry, and other unaccounted factors reaches maximum acceleration of about $1.5 \cdot 10^{-6}$ m/s^2 (as depicted in Fig. 5), the solar sail control variables alter (Fig. 6) when applying the developed control strategy.

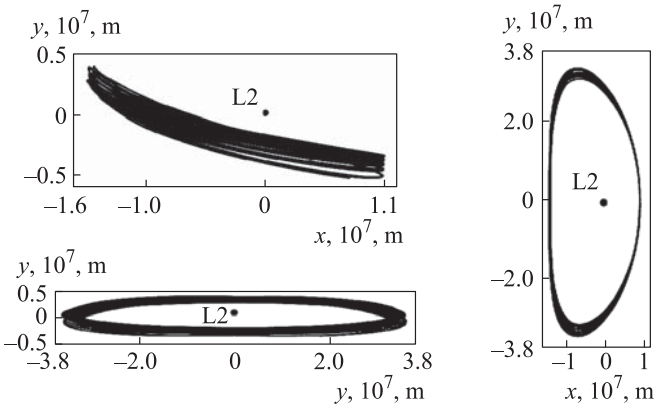

Fig. 6. Alteration in disturbance acceleration acting on the spacecraft

Based on Fig. 5, it could be concluded that the developed high-precision model of spacecraft dynamics, along with the method for establishing a reference orbit, successfully finalizes the reference orbit design for a spacecraft equipped with the solar sail. Parameters are outlined in (5) and above. Furthermore, Fig. 7 indicates that the developed orbit keeping strategy efficiently guarantees orbital stability in the presence of disturbances outlined in Fig. 6.

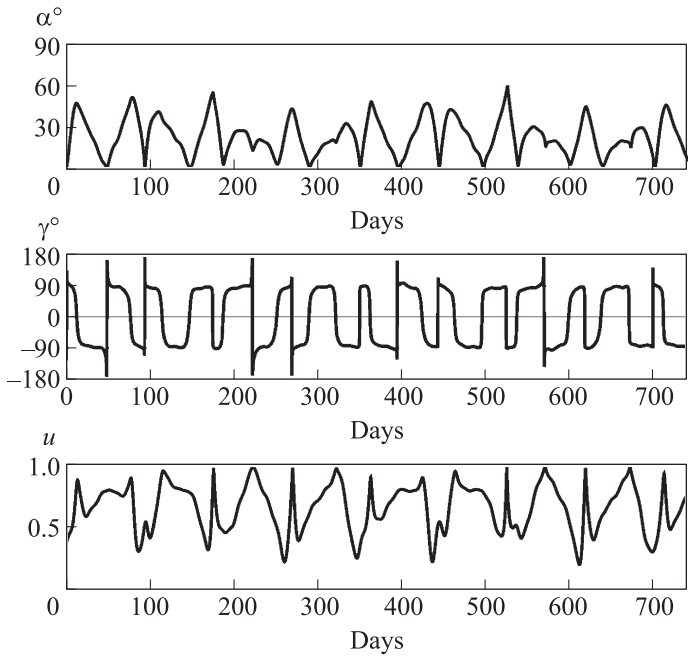

Fig. 7. Alteration in the solar sail control variables

Discussion of the results obtained. Compared to the *Queqiao-1* relay satellite, which uses traditional chemical rocket engines, the solar sail satellites have certain advantages.

1. *Reduced weight*. With a similar orbital support capability, the solar sail mass is by 66 % less than the orbit keeping fuel mass of *Queqiao-1*. At the same time, structural mass of the solar sail control system is also less than the total mass of the fuel tank, fuel supply system, engine and other components, according to the engineering experience. Moreover, a solar sail could control a transfer from the Earth orbit to the Moon orbit, which requires more time but less fuel mass.

2. *Accurate orbit keeping*. Unlike the intermittent-pulse orbit control strategy used by a satellite with the traditional engines, the orbit control strategy applied by a solar sail satellite implements the real-time attitude control, and ensures high precision in the orbit keeping. This creates better conditions for satellite positioning and signal transmission.

3. *Extended operating time*. *Queqiao-1's* in-orbit operating time is extended to 9 years by introducing the high-accuracy control technology. However, the potential in-orbit operating time of a solar sail satellite would significantly exceed this indicator, because flight control characteristics of the solar sail remain virtually unchanged over time.

Summary. This work proves feasibility and efficiency of using a solar sail to establish and keep the orbit of an Earth–Moon relay satellite. Modern technologies in the development, construction and control of the solar sails are significantly superior to those of *Ikaros*, but at its technical level, it is also possible to create a relay satellite with the solar sail, which has advantages over a similar satellite equipped with the traditional engine. Until now, the main research on using a solar sail was focused on the deep space exploration, but the Moon exploration projects represent more urgent, supported, and rewarding tasks. Solar sail application on board the Earth–Moon relay satellite would significantly improve practical value and pace of technological evolution in the solar sail technology. However, it should be noted that the technology of solar sail control mechanics is still in its development stage. When using a solar sail for flight control, limitations such as accuracy and responsiveness of the control mechanics should be taken into account.

REFERENCES

[1] Heidmann J. A proposal for a radio frequency interference-free dedicated lunar far side crater for high sensitivity radioastronomy: programmatic issues. *Acta Astronaut.*, 2000, vol. 46, no. 8, pp. 555–558. DOI: https://doi.org/10.1016/S0094-5765(00)00002-3

[2] Li S., Lucey P.G., Milliken R.E., et al. Direct evidence of surface exposed water ice in the lunar polar regions. *PNAS*, 2018, vol. 115, no. 36, pp. 8907–8912. DOI: https://doi.org/10.1073/pnas.1802345115

[3] Binder A.B. Lunar prospector: overview. *Science*, 1998, vol. 281, no. 5382, pp. 1475–1476. DOI: https://doi.org/10.1126/science.281.5382.1475

[4] Robinson M.S., Brylow S.M., Tschimmel M., et al. Lunar reconnaissance orbiter camera (LROC) instrument overview. *Space Sc. Rev.*, 2010, vol. 150, no. 1, pp. 81–124. DOI: https://doi.org/10.1007/s11214-010-9634-2

[5] Colaprete A., Elphic R.C., Heldmann J., et al. An overview of the lunar crater observation and sensing satellite (LCROSS). *Space Sc. Rev.*, 2012, vol. 167, no. 1, pp. 3–22. DOI: https://doi.org/10.1007/s11214-012-9880-6

[6] Kato M., Sasaki S., Takizawa Y., et al. The Kaguya mission overview. *Space Sc. Rev.*, 2010, vol. 154, no. 1, pp. 3–19. DOI: https://doi.org/10.1007/s11214-010-9678-3

[7] Dachev T.P., Tomov B.T., Matviichuk Y.N., et al. An overview of RADOM results for Earth and Moon radiation environment on Chandrayaan-1 satellite. *Adv. Space Res.*, 2011, vol. 48, no. 5, pp. 779–791. DOI: https://doi.org/10.1016/j.asr.2011.05.009

[8] Sweetser T.H., Broschart S.B., Angelopoulos V., et al. ARTEMIS mission design. In: *The ARTEMIS Mission*. Cham, Springer Nature, 2014, pp. 61–91.
DOI: https://doi.org/10.1007/978-1-4614-9554-3_4

[9] Xu L., Li H., Pei Z., et al. A brief introduction to the international lunar research station program and the interstellar express mission. *Chin. J. Space Sc.*, 2022, vol. 42, no. 4, pp. 511–513. DOI: https://doi.org/10.11728/cjss2022.04.yg28

[10] Zhdanov V.L. [Russian-Chinese international cooperation in the field of space exploration]. *Fundamentalnye i prikladnye nauchnye issledovaniya: aktualnye voprosy, dostizheniya i innovatsii. Sb. st. LXII Mezhdunar. nauch.-prakt. konf.* [Fundamental and applied scientific research: topical issues, achievements and innovations. Proc. LXII Int. Sc.-Pract. Conf.]. Penza, Nauka i Prosveshchenie Publ., 2022, pp. 313–315 (in Russ.).
EDN: ORPSJZ

[11] Lihua Z., Liang X., Ji S., et al. One year on-orbit operation of queqiao lunar relay communications satellite. *Aerospace China*, 2019, vol. 20, no. 3, pp. 5–13.
DOI: https://doi.org/10.3969/j.issn.1671-0940.2019.03.001

[12] Folta D., Woodard M., Cosgrove D. Stationkeeping of the first Earth–Moon libration orbiters: the ARTEMIS mission. *AAS/AIAA Astrodynamics Specialist Conf.*, 2011, vol. 142, pp. 1697–1715.

[13] Lei L., Jianfeng C., Songji H., et al. Maintenance of relay orbit about the Earth–Moon collinear libration points. *Journal of Deep Space Exploration*, 2015, vol. 2, no. 4, pp. 318–324. DOI: https://dx.doi.org/10.15982/j.issn.2095-7777.2015.04.004

[14] Gao S., Zhou W.Y., Zhang L., et al. Trajectory design and flight results for Change 4-relay satellite. *Sc. Sin. Technol.*, 2019, vol. 49, no. 2, pp. 156–165.
DOI: https://doi.org/10.1360/N092018-00393

[15] Jianfeng D., Xie L., Cuilan L., et al. Orbit determination and analysis of Chang'E-4 relay satellite on mission orbit. *Journal of Deep Space Exploration*, 2019, vol. 6, no. 3, pp. 247–253. DOI: https://dx.doi.org/10.15982/j.issn.2095-7777.2019.03.008

[16] Tsuda Y., Mori O., Funase R., et al. Achievement of IKAROS — Japanese deep space solar sail demonstration mission. *Acta Astronaut.*, 2013, vol. 82, no. 2, pp. 183–188.
DOI: https://doi.org/10.1016/j.actaastro.2012.03.032

[17] Zhao J., Tian Q., Hu H.Y. Deployment dynamics of a simplified spinning IKAROS solar sail *via* absolute coordinate-based method. *Acta Mech. Sin.*, 2013, vol. 29, no. 1, pp. 132–142. DOI: https://doi.org/10.1007/s10409-013-0002-9

[18] Yu W., Starinova O.L. Study on displaced orbits below the Moon's south pole near l2 point based on solar sail. *Mekhatronika, Avtomatizatsiya, Upravlenie*, 2023, vol. 24, no. 12, pp. 652–659. DOI: https://doi.org/10.17587/mau.24.652-659

[19] Yu W., Wu K. [Characteristics and method of maintaining the motion of a solar sail in a halo orbit near point L2 in the Earth–Moon system]. *Aviatsiya i kosmonavtika. Tez. 20 Mezhdunar. konf.* [Aviation and Cosmonautics. Abs. 20th Int. Conf.]. Moscow, Pero Publ., 2021, pp. 372–374 (in Russ.). EDN: TTSTFY

[20] Khabibullin R.M., Starinova O.L. An analysis of guided motion of a research spacecraft with a solar sail. *Izvestiya vysshikh uchebnykh zavedeniy, Mashinostroyeniye* [BMSTU Journal of Mechanical Engineering], 2019, no. 12, pp. 94–103 (in Russ.).
DOI: http://dx.doi.org/10.18698/0536-1044-2019-12-94-103

[21] Bray T.A., Gouclas C.L. Doubly symmetric orbits about the collinear Lagrangian points. *Astron. J.*, 1967, no. 72, pp. 202–213. DOI: https://doi.org/10.1086/110218

[22] Breakwell J.V., Brown J.V. The 'halo' family of 3-dimensional periodic orbits in the Earth–Moon restricted 3-body problem. *Celest. Mech.*, 1979, vol. 20, no. 4, pp. 389–404.
DOI: https://doi.org/10.1007/BF01230405

[23] Howell K.C. Families of orbits in the vicinity of the collinear libration points. *J. Astronaut. Sc.*, 2001, vol. 49, pp. 107–125. DOI: https://doi.org/10.1007/BF03546339

[24] Chunzhui D., Fain M.K., Starinova O.L. Analysis and design of halo orbits in cislunar space. *IOP Conf. Ser.: Mater. Sc. Eng.*, 2020, vol. 984, pp. 12–33.
DOI: https://doi.org/10.1088/1757-899X/984/1/012033

Yu W. — Cand. Sc. (Eng.), Department of Flight Dynamics and Control Systems, Samara National Research University (Moskovskoe shosse 34, Samara, 443086 Russian Federation).

Starinova O.L. — Dr. Sc. (Eng.), Professor, Head of the Department of Flight Dynamics and Control Systems, Samara National Research University (Moskovskoe shosse 34, Samara, 443086 Russian Federation).

Please cite this article as:

Yu W., Starinova O.L. Flight control in a halo orbit in vicinity of the L2 point in the Earth–Moon system using a solar sail. *Herald of the Bauman Moscow State Technical University, Series Mechanical Engineering*, 2025, no. 2 (153), pp. 70–83.
EDN: OWONJP